

Crosstalk in automultiscopic 3-D displays: Blessing in disguise?

Ashish Jain and Janusz Konrad

Department of Electrical and Computer Engineering, Boston University
8 Saint Mary's Street, Boston, MA 02215

ABSTRACT

Most of 3-D displays suffer from interocular crosstalk, i.e., the perception of an unintended view in addition to intended one. The resulting “ghosting” at high-contrast object boundaries is objectionable and interferes with depth perception. In automultiscopic (no glasses, multiview) displays using microlenses or parallax barrier, the effect is compounded since several unintended views may be perceived at once. However, we recently discovered that crosstalk in automultiscopic displays can be also beneficial. Since spatial multiplexing of views in order to prepare a composite image for automultiscopic viewing involves sub-sampling, prior anti-alias filtering is required. To date, anti-alias filter design has ignored the presence of crosstalk in automultiscopic displays. In this paper, we propose a simple multiplexing model that takes crosstalk into account. Using this model we derive a mathematical expression for the spectrum of single view with crosstalk, and we show that it leads to reduced spectral aliasing compared to crosstalk-free case. We then propose a new criterion for the characterization of ideal anti-alias pre-filter. In the experimental part, we describe a simple method to measure optical crosstalk between views using digital camera. We use the measured crosstalk parameters to find the ideal frequency response of anti-alias filter and we design practical digital filters approximating this response. Having applied the designed filters to a number of multiview images prior to multiplexing, we conclude that, due to their increased bandwidth, the filters lead to visibly sharper 3-D images without increasing aliasing artifacts.

Keywords: 3-D automultiscopic displays, interocular crosstalk, anti-alias filtering

1. INTRODUCTION

Interocular crosstalk perceived by viewers of 3-D displays induces ghosting at the boundaries of high-contrast objects with non-zero screen parallax.¹ This ghosting is detrimental to the 3-D experience as it often leads to difficulties with 3-D fusion, eye strain, even headaches. Methods reducing interocular crosstalk have been devised for stereoscopic displays in the past,²⁻⁴ but the problem is much more complex for multiview displays.

The interocular crosstalk is always caused by some physical process on which the separation of views relies (e.g., optical, mechanical, electrical). In lenticular multiview displays, of interest here, it is caused by optical properties of the lenticular sheet. It is worth noting, however, that had the optics been perfect (e.g., the point spread function of each lenticule were the Dirac impulse) the perceived 3-D image brightness would have been much lower as only light from a single view would have been perceived with pixels for other views being blanked out. In this sense, crosstalk is somewhat beneficial since it increases light output and perceived resolution of the screen.⁵ This observation leads to the following question: Can the fact that light from unintended views, in addition to the light from an intended view, is perceived by viewers be also beneficial from the standpoint of view multiplexing and related pre-processing?

As recently shown, prior to multiplexing views in order to prepare a composite image for display on a lenticular (or parallax-barrier) 3-D screen, suitable low-pass filtering is required.⁶⁻⁸ That filtering removes high-frequency details from individual views since otherwise sub-sampling, an inherent step in view multiplexing, would lead to aliasing perceived as color fringing at sharp object boundaries, Moire patterns, granular noise, etc. However, the simple sub-sampling model used to date ignores the optical crosstalk effects present in lenticular and parallax-barrier multiview displays.

In this paper, we consider the impact of crosstalk in spatially-multiplexed automultiscopic 3-D displays on optimal view multiplexing and, in particular, on anti-alias filter design. First, we propose a simple linear model for view multiplexing accounting for optical inter-view crosstalk. We then derive a mathematical expression for

the spectrum of a single perceived view accounting for optical crosstalk. As it turns out, spectral replications, due to the implicit sub-sampling, are of unequal gain unlike in the absence of crosstalk. In order to account for the unequal gains, we propose a new criterion for the characterization of aliasing; instead of equidistant 2-D frequency partitioning, we propose partitioning based on equal spectral power. We quantify the spectral power of individual views using a common autocorrelation model for Markov-1 sources, and show that accounting for optical crosstalk leads to increased bandwidth of the ideal anti-alias filter. In the experimental part, we describe a simple method to measure the optical crosstalk between views using digital camera. We then use the measured crosstalk parameters to find an ideal frequency response of anti-alias filter and we design a practical digital anti-alias filter approximating this response. We apply the designed filter to a number of multiview images prior to multiplexing, and in informal subjective tests we conclude that, due to their increased bandwidth, the filters lead to visibly sharper 3-D images while not increasing aliasing artifacts.

2. SPATIALLY-MULTIPLEXED AUTOMULTISCOPIC 3-D DISPLAYS

Binocular perception can be accomplished by means of view separation either using eyewear or without it. Stereoscopic systems employing eyewear are based on the principles of wavelength filtering, light polarization, or temporal shuttering. Stereoscopic systems void of eyewear, also called *autostereoscopic*, employ spatial view multiplexing and rely on an on-screen view selection mechanism, typically microlens sheet or parallax barrier. Stereoscopic displays allow only two views from any position in front of the screen thus resulting in a conflict between motion and parallax (static objects tend to rotate on screen with viewer head motion).

In order to combat the motion-parallax conflict of two-view systems, multiview, or *multiscopic*, 3-D displays have been developed. A synchronism between motion and parallax can be accomplished through viewer head tracking, based on which proper view pairs are rendered (*active automultiscopic* 3-D displays), through spatial multiplexing of all views and reliance on microlenses/parallax barrier to project individual views into separate viewing zones (*spatially-multiplexed automultiscopic* 3-D displays), or through other means.⁹ Although in this paper we are interested in lenticular spatially-multiplexed automultiscopic 3-D displays,¹⁰⁻¹² and the experimental results presented are for 9-view *SynthaGramTMSG202* monitor (20-in, 1600×1200 LCD panel) from StereoGraphics Corp., our considerations apply equally to other view selection technologies based on spatial multiplexing.^{13,14}

The spatially-multiplexed automultiscopic 3-D displays we consider have a transparent sheet composed of very thin semi-cylindrical microlenses (lenticules) placed in front of a pixel-addressable screen, such as an LCD or plasma panel.¹⁵ The lenticular sheet is designed and placed in such a way that the screen surface is at focal length of the microlenses, and both are carefully aligned to minimize optical interference. While early autostereoscopic (two-view) displays had the lenticules aligned with pixel columns (each lens typically covered one column of pixels), the newer multiview displays have lenticules oriented at a small angle to pixel columns.¹⁶ The slanted lenticule arrangement better balances effective 3-D resolution between vertical and horizontal directions and, with a careful angle selection, reduces Moiré patterns resulting from black (dead) space between pixels seen through the lenses. At the same time, however, it makes pixels visible from one viewpoint laid out in a semi-irregular pattern. Fig. 5(a) shows a typical pattern for red image component; small dots represent screen raster, while red crosses represent those pixels that have been assigned a value from red component of view #1. Note that at each pixel, only one color component is allowed for a given view (color components are considered co-located). Clearly, the sub-sampling pattern of a color component is semi-irregular but belongs to the screen raster (orthonormal lattice). For a more detailed discussion of automultiscopic display rasters, the reader is encouraged to consult our previous work⁸ and papers by van Berkel *et al.*^{10,17}

A problem that received little attention to date is optical crosstalk in spatially-multiplexed automultiscopic displays. In practice, a viewer in front of the screen will see light from the intended view *and* also some light from other views whose pixels are adjacent to intended-view pixels. This light leakage, caused by lenticule properties, is perceptually detrimental since it induces interocular crosstalk that often manifests itself as double contours (ghosting) at high-contrast edges. At the same time, optical crosstalk is beneficial as it assures smooth transition between views, and increases perceived display resolution and brightness (seeing light from the intended view only on an N -view display, would have cut light output N -fold).⁵ Thus, of interest is quantification of optical crosstalk, its inclusion in multiplexing models, and subsequent crosstalk-aware design of anti-alias filters.

3. CROSSTALK-AWARE VIEW MULTIPLEXING MODEL

In this section, we propose a simple linear model for view multiplexing that accounts for crosstalk between the views. While multiplexing N views into a single image to be displayed on a screen, certain R , G , and B sub-pixels are extracted from each view by means of 2-D sub-sampling. This sub-sampling process can be modeled by the multiplication of original view samples by a discrete bi-sequence of 2-D Kronecker delta impulses.¹⁸ However, in order to keep the notation simple, and facilitate convincing visualization of the proposed model, we will restrict the discussion in this and next section section to 1-D case; the discussed principles apply to 2-D, but the notation is more complex and visualization more cumbersome. Therefore, we assume for now that multiplexing, and thus sub-sampling, occurs only horizontally and is regular, i.e., that for a given view its sub-pixels have the same neighbors (the same views) throughout the image domain. Note that the spectral analysis, anti-alias filter design and actual experiments on images in later sections will be performed in 2-D.

Let $u_k[n]$ be a 1-D discrete-space signal, e.g., one row of red sub-pixels from view number k . The sub-sampling of $u_k[n]$ by a factor of N can be modeled by its multiplication with a train of impulses defined as follows:

$$x[n] = \sum_{l=-\infty}^{+\infty} \delta[n - lN], \quad n \in Z, \quad (1)$$

where $\delta[n]$ is a 1-D Kronecker delta impulse ($\delta[n]$ equals 1 for $n = 0$ and 0 otherwise). Note that the sub-sampling factor N equals the number of views the automultiscopic screen can display so that after $N:1$ sub-sampling N views multiplexed together constitute a displayable image of resolution identical to that of each original view. The train of impulses $x[n]$ is shown in Fig. 1(a).

Clearly, the multiplication of $u_k[n]$ by $x[n]$ results in samples from view number k only (intended view). In order to incorporate crosstalk into this model, in addition to samples from u_k samples from other views, e.g., u_{k-1} or u_{k+1} , must appear at the output of the multiplier. This can be accomplished by including additional impulses with magnitudes equal to crosstalk coefficient a defined as a ratio of light energy of unintended view to the light energy of intended view, both displaying the same image. In other words, the perceived sampling in this case can be represented as the sum of impulse trains with different amplitudes and phase shifts.

If we assume that the number of views N is odd, as is the case for our *SynthaGramTM* monitor, then for the central view u_M , where $M = (N + 1)/2$, we may have crosstalk from up to $M - 1$ views on each side. If the central view u_M is the intended view, then we let the crosstalk coefficients for views u_{M+1} , u_{M+2} , ..., u_{2M-1} bleeding into view number M be a_1, a_2, \dots, a_{M-1} , respectively. Assuming that crosstalk into an intended view from spatially-symmetric views is the same, the crosstalk coefficients for views $M - 1$, $M - 2$, ..., 1 bleeding into view number M are also a_1, a_2, \dots, a_{M-1} , respectively. It is also assumed that the intended view u_M is seen at full brightness implying that $a_0 = 1$, whereas $0 \leq a_k < 1$ for $k \neq M$.

Thus, the sub-sampling sequence for view u_M , i.e., intended view seen at full brightness, is the same as for the no crosstalk case (1):

$$x_M[n] = \sum_{l=-\infty}^{+\infty} \delta[n - lN]. \quad (2)$$

However, the sub-sampling sequences for other views bleeding into view number M have non-unit gains and can be expressed as follows:

$$\begin{aligned} x_{M-1}[n] &= a_1 \sum_{l=-\infty}^{+\infty} \delta[n - lN - 1], & x_{M+1}[n] &= a_1 \sum_{l=-\infty}^{+\infty} \delta[n - lN + 1] \\ x_{M-2}[n] &= a_2 \sum_{l=-\infty}^{+\infty} \delta[n - lN - 2], & x_{M+2}[n] &= a_2 \sum_{l=-\infty}^{+\infty} \delta[n - lN + 2] \\ x_1[n] &= a_{M-1} \sum_{l=-\infty}^{+\infty} \delta[n - lN - M + 1], & x_{2M-1}[n] &= a_{M-1} \sum_{l=-\infty}^{+\infty} \delta[n - lN + M - 1] \end{aligned} \quad (3)$$

The contribution of all pixels, i.e., from the intended as well as unintended views, to the *perception* of view number M can be modeled as sub-sampling of the *multiplexed* image by the following train of impulses:

$$x_{all}[n] = x_1[n] + x_2[n] + \dots + x_{2M-1}[n] \quad (4)$$

An example a train of impulses for sub-sampling with crosstalk is shown in Fig 1(b).

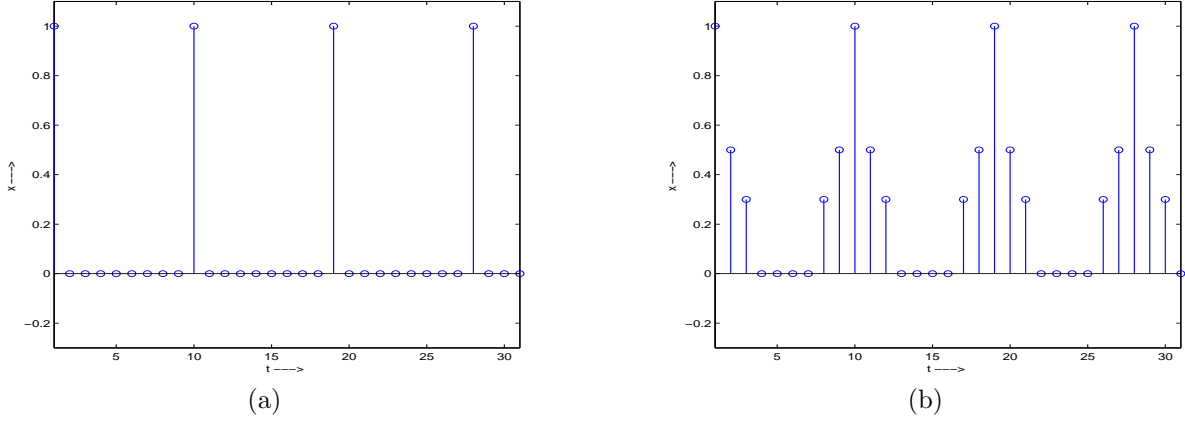


Figure 1. Train of impulses for sub-sampling: (a) without crosstalk, $x[n]$; and (b) with crosstalk, $x_{all}[n]$ ($N = 9, a_1 = 0.5, a_2 = 0.3, a_3 = a_4 = 0$).

It is very instructive to consider spectral implications of the above sampling models without and with crosstalk. The discrete-space Fourier transform of the train of unit impulses (1) can be shown to equal:

$$X(\omega) = \mathcal{F}\{x[n]\} = \frac{2\pi}{N} \sum_{k=-\infty}^{+\infty} \delta\left(\omega - \frac{2\pi}{N}k\right),$$

where $\delta(\cdot)$ is the Dirac delta function (note the regular parentheses instead of square brackets used for the Kronecker delta). Derivation of the above formula is beyond the scope of this paper, but can be easily deduced from standard formulas given in digital signal processing textbooks (e.g., Table 3.3 and equation (13.12) in Mitra's "Digital Signal Processing"¹⁹). The above equation can be re-written in terms of frequencies instead of angular frequencies as follows:

$$X(f) = \frac{1}{N} \sum_{k=-\infty}^{+\infty} \delta\left(f - \frac{k}{N}\right) \quad (5)$$

Note that, similarly to $x[n]$, $X(f)$ is a train of impulses of equal amplitude.

Similarly, the Fourier transform of $x_{all}[n]$ can be written as follows:

$$X_{all}(f) = \frac{1}{N} \sum_{k=-\infty}^{+\infty} \delta\left(f - \frac{k}{N}\right) [1 + 2a_1 \cos(2\pi f) + 2a_2 \cos(4\pi f) + \dots + 2a_{M-1} \cos((M-1)2\pi f)], \quad (6)$$

where the $\cos(\cdot)$ terms are due to symmetry between x_{M-1} and x_{M+1} , x_{M-2} and x_{M+2} , and so on. Note that for $f = 0$ all the cosine terms are in phase:

$$X_{all}(0) = \frac{1}{N} [1 + 2a_1 + 2a_2 + \dots + 2a_{M-1}],$$

and thus the spectrum at DC has high gain. On the other hand, the closest spectral replication at $f = \frac{1}{N}$ is not in phase as not all cosine terms are positive:

$$X_{all}(1/N) = \frac{1}{N} \left[1 + 2a_1 \cos\left(\frac{2\pi}{N}\right) + 2a_2 \cos\left(\frac{4\pi}{N}\right) + \dots + 2a_{M-1} \cos\left((M-1)\frac{2\pi}{N}\right) \right].$$

Clearly, $X_{all}(f)$ is also a train of impulses, with the baseband impulse located at $f = 0$ (DC) and its nearest neighbors located at $f = \pm \frac{1}{N}$. The impulses, however, are of different amplitudes due to crosstalk. Since the baseband impulse has greater gain than impulses at $f = \pm \frac{1}{N}$, it can be expected that the sub-sampled signal will have different spectrum than for the case with no crosstalk where all spectral impulses have the same amplitude.

The above discussion is easier to follow when considering plots in Fig. 2 for the case of $N = 3$ views. The value of M is 2 in this case, and we chose the crosstalk coefficient $a_1 = 0.6285$. Clearly, while in the case without crosstalk all impulses have the same amplitude, in the case accounting for crosstalk the amplitude of nearest off-DC impulses is only 16.5% of the baseband impulse.

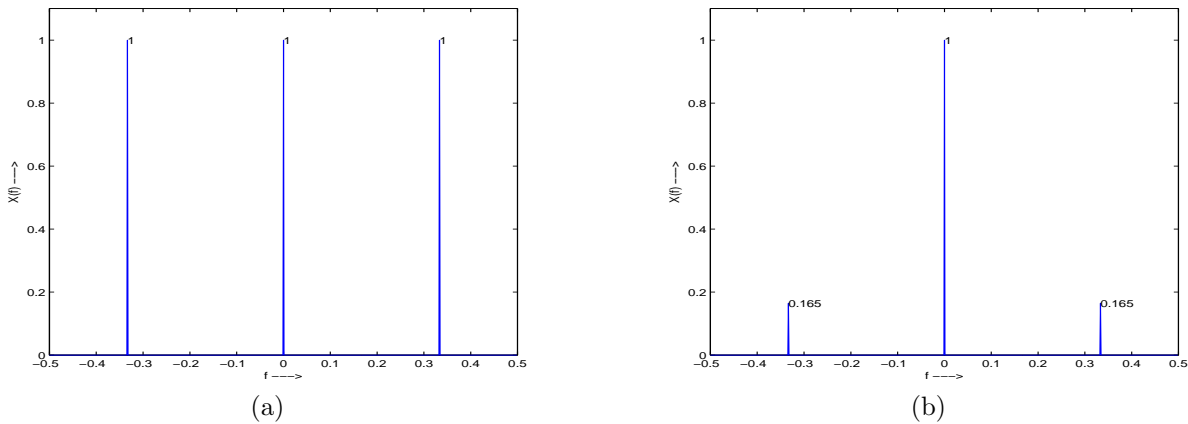


Figure 2. Discrete-space Fourier transform of sub-sampling sequence: (a) $X(f)$, without crosstalk (1), and (b) $X_{all}(f)$, with crosstalk (4) for $N = 3$ and $a_1 = 0.6285$. The maximum amplitude of each sequence has been normalized to 1.

4. COMPUTING FREQUENCY SPECIFICATIONS OF IDEAL ANTI-ALIAS FILTER

As discussed in the previous section, sub-sampling of signal $u_k[n]$ is accomplished by multiplication with the train of impulses $x[n]$, and this leads to convolution in the frequency domain:

$$\hat{u}_k[n] = u_k[n]x[n] \quad \xleftrightarrow{\mathcal{F}} \quad \hat{U}_k(f) = U_k(f) * X(f), \quad (7)$$

where $\hat{u}_k[n]$ is the sub-sampled signal, $\hat{U}_k(f) = \mathcal{F}\{\hat{u}_k[n]\}$ is its Fourier transform, while $U_k(f)$ and $X(f)$ are Fourier transforms of $u_k[n]$ and $x[n]$, respectively. Since $X(f)$ is a unit impulse train (equation (1) and Fig. 2(a)), its convolution with signal spectrum $U_k(f)$ results in replication of this spectrum at impulse locations of $X(f)$. Thus, the case of no crosstalk is the standard case of sub-sampling where identical spectra are replicated at locations $k/N, k \in \mathcal{Z}$ on the normalized frequency axis. It is easy to identify the bandwidth of the optimal anti-alias filter in this case; its cut-off frequency is simply the midpoint between DC and the nearest spectral replication (since both spectra have the same gain), namely $f_c = 1/(2N)$ or $\omega_c = \pi/N$ in our case.

However, in the case of model with crosstalk the situation is different. Let's assume for simplicity of the subsequent argument that all views are identical and so are their spectra. Then, the multiplexed image is identical to one of the views, e.g., $u_k[n]$, and the case of multiplexing model with crosstalk can be expressed by equation (7) with $x_{all}[n]$ and $X_{all}(f)$ replacing $x[n]$ and $X(f)$, respectively. Thus, again spectral replications will result but with different gains that depend on the train of impulses $X_{all}(f)$ as demonstrated in Fig. 2. Since the gains for neighboring spectral replications may be quite different, the previous mid-point frequency argument to determine optimal filter cut-off frequency applies no more; we need to know the image spectrum. Instead of designing an optimal anti-alias filter for a specific image, which is not impossible, we propose to use an image model to statistically parameterize the image and its spectrum.

We propose to use the first-order, 1-D Markov model (the so-called Markov-1 model) often used to describe images along scan lines.²⁰ This model's autocorrelation function, that expresses average similarity between

pixels (the larger the autocorrelation the more similar the pixels), is the following exponential function:

$$R_u[m] = \rho^{|m|}, \quad (8)$$

where $0 < \rho < 1$ is a correlation coefficient, usually in 0.9-0.99 range. Clearly, as m increases the autocorrelation $R_u[m]$ drops. For images, also a 2-D separable exponential function is often used.

The Fourier transform of a 1-D exponential function is:

$$\mathcal{F}\{e^{-2\pi f_0|x|}\} = \frac{1}{\pi} \frac{f_0}{f^2 + f_0^2}. \quad (9)$$

Using equations (8) and (9), we compute the power spectral density (Fourier transform of autocorrelation $R_u[m]$) of the 1-D signal:

$$\Phi(f) = \mathcal{F}\{\rho^{|m|}\} = \frac{1}{\pi} \frac{f_0}{f^2 + f_0^2} \quad (10)$$

where $f_0 = -(\ln \rho)/(2\pi)$. As frequency f increases, the power spectral density $\Phi(f)$ gets smaller.

We use $\Phi(f)$ to model the spectrum of each view (all views are assumed identical), and thus the overall spectrum of multiplexed views in the absence of crosstalk can be expressed as $\Phi(f) * X(f)$ and in the presence of crosstalk – as $\Phi(f) * X_{all}(f)$. Fig. 3 shows both spectra for autocorrelation coefficient $\rho = 0.9$. Note the lower amplitude of the off-DC spectra for the case of model with crosstalk. Since the impact of these lower-amplitude spectra on the baseband spectrum at DC will be less than for the case without crosstalk, in order to maintain the same level of aliasing (spectral energy leak) in both cases it is possible to employ a larger bandwidth filter in the case of model with crosstalk. The question is how to determine the bandwidth of such a filter?

As is clear from equations (5) and (6), as well as Figs. 2 and 3, replications of the spectrum occur at frequencies $f = \pm k/N, k \in Z$. For the above autocorrelation model, the mathematical expression for spectral replication at $f = 0$ is $\pi \frac{f_0}{f^2 + f_0^2}$. Similarly, a replication at $f = 1/N$ is $\pi \frac{A f_0}{(f - 1/N)^2 + f_0^2}$, where A is a spectrum gain resulting from the convolution of $\Phi(f)$ with the impulse train (Fig. 2). For the model with no crosstalk $A = 1$, but for the model with crosstalk A is defined as follows:

$$A = \frac{X_{all}(f)_{f=\frac{1}{N}}}{X_{all}(f)_{f=0}}.$$

In order to minimize aliasing from repeat spectra, while maximally preserving spectral content of the original signal, we propose to define the cut-off frequency f_c of the anti-alias filter as a frequency at which the repeat spectrum equals the baseband spectrum (assuming more distant repeat spectra make no contribution), expressed as follows:

$$\frac{f_0}{f_c^2 + f_0^2} = \frac{A f_0}{(f_c - \frac{1}{N})^2 + f_0^2}. \quad (11)$$

Solving for f_c , we obtain the following cut-off frequency:

$$f_c = \frac{2/N \pm \sqrt{(2/N)^2 - 4(1-A)((1/N)^2 + (1-A)f_0^2)}}{2(1-A)}.$$

It is easy to check, using de l'Hôpital's rule, that for $A = 1$, $f_c = 1/(2N)$, as expected for the crosstalk-free case. It can be also verified that for $A < 1$, $f_c > 1/(2N)$, and thus the anti-alias filter bandwidth increases for the case with crosstalk.

We demonstrate this by an example. Assume there are $N = 3$ views, with crosstalk coefficient $a_1 = 0.6285$, and let us choose $\rho = 0.9$. For these specifications, we have $A = 0.1646$ and $f_0 = 0.0168$. The spectrum of sampled signal under no crosstalk and with crosstalk assumptions is shown in Fig. 3. Solving the above equations for anti-alias filter cut-off frequency we get $f_c = 1/4.20$ for the model with crosstalk which is significantly larger than $f_c = 1/6$ without crosstalk.

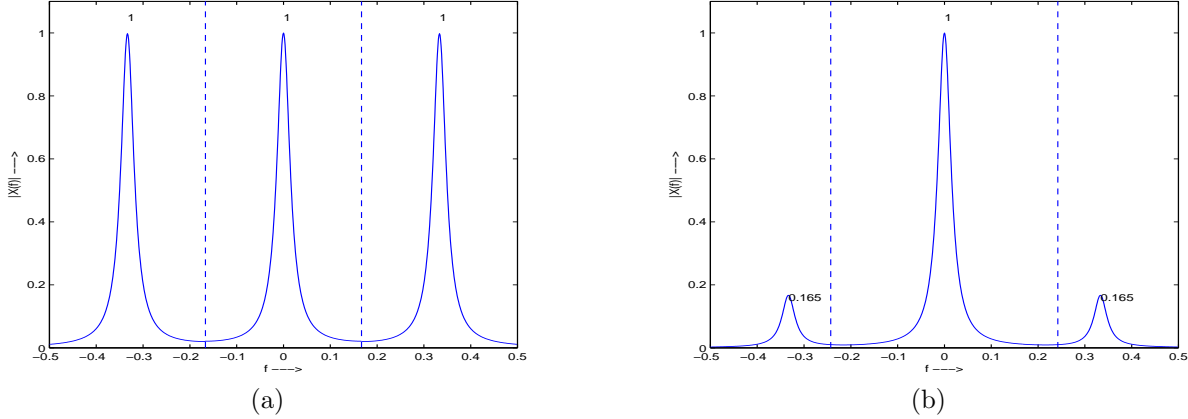


Figure 3. Baseband spectrum and nearest repeat spectra: (a) without crosstalk, $f_c = 0.17$; (b) with crosstalk, $f_c = 0.24$.

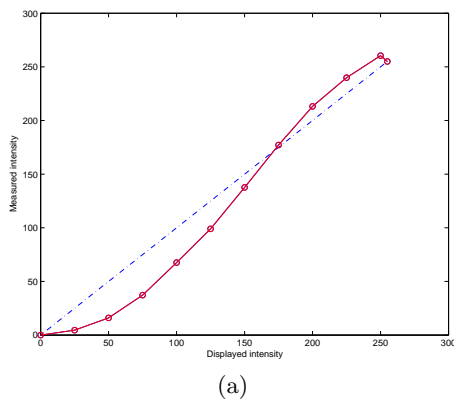
5. EXPERIMENTAL RESULTS

5.1. Crosstalk measurement for a lenticular display

In order to measure crosstalk coefficients (a_1, a_2, \dots), we used a digital camera placed in front of *SynthaGram*TM SG202 display in a darkroom (no other light sources) at such a distance that active screen area fully covered camera's field of view. We computed mean squared intensity of three color components from each captured image. The screen with all views turned off (black) was captured first to create a reference for the crosstalk calculation. The camera was set to manual mode to keep the aperture and focal length constant during measurements.

Since we were to measure a range of intensities, we first needed to verify linearity of our measurement system. We performed the following steps:

1. Apply maximum intensity (255) to view #1 to produce a uniform white image while keeping other views black (0) and manually adjust angular camera position to capture the maximum amount of light.
2. Vary intensity of view #1 from 0 to 255, and for each intensity level capture the light emitted by the screen (mean-squared value) using the camera.
3. Plot the captured light intensity against the actual display intensity (Fig. 4(a)).



(a)

| | 1 | 2 | 3 | 4 | 5 | 6 | 7 | 8 | 9 |
|---|---|-------|-------|-------|-------|-------|-------|-------|-------|
| R | 1 | 0.628 | 0.128 | 0.010 | 0.004 | 0.004 | 0.010 | 0.117 | 0.589 |
| G | 1 | 0.665 | 0.159 | 0.015 | 0.005 | 0.005 | 0.014 | 0.132 | 0.596 |
| B | 1 | 0.683 | 0.173 | 0.016 | 0.004 | 0.004 | 0.013 | 0.134 | 0.596 |
| Y | 1 | 0.656 | 0.151 | 0.014 | 0.004 | 0.004 | 0.012 | 0.127 | 0.594 |

(b)

| | 1 | 2 | 3 | 4 | 5 | 6 | 7 | 8 | 9 |
|---|-------|-------|---|-------|-------|-------|-------|-------|-------|
| R | 0.093 | 0.598 | 1 | 0.640 | 0.143 | 0.013 | 0.006 | 0.006 | 0.011 |
| G | 0.112 | 0.608 | 1 | 0.667 | 0.172 | 0.017 | 0.005 | 0.005 | 0.012 |
| B | 0.114 | 0.618 | 1 | 0.678 | 0.186 | 0.017 | 0.004 | 0.004 | 0.012 |
| Y | 0.106 | 0.605 | 1 | 0.660 | 0.164 | 0.015 | 0.005 | 0.004 | 0.011 |

(c)

Figure 4. (a) Camera-captured versus actual screen intensity; and measured crosstalk ratio for: (b) view #1; and (c) view #3.

From the plot in Fig. 4(a) we can assume that our setup to measure the crosstalk is reasonably linear except at the extreme end of the intensity range. We then performed crosstalk measurement as follows:

1. Apply maximum intensity to a selected view, while keeping other views black, and manually adjust angular camera position to capture the maximum amount of light.
2. Apply maximum intensity individually to each view (one at a time), while keeping other views black, and capture the light emitted by the screen using the camera.
3. Perform steps 1 and 2 for different views.

The crosstalk measurement results for views #1 and #3 are shown in Fig. 4(b) and 4(c). Based on these results we conclude that:

1. The amounts of crosstalk for three primary colors (red, green and blue) are approximately equal. Thus, we can design an anti-alias filter for one color only.
2. The crosstalk is approximately symmetric spatially. For example, for view #1 the amount of crosstalk from view #2 and view #9 is comparable, as it is for views #3 and #8, #4 and #7, #5 and #6. A similar observation can be made for view #3.
3. The crosstalk between two views is a function of distance between them. For example, views #1 and #2 have the same degree of crosstalk as views #3 and #4. Similarly, crosstalk between views #1 and #3 has the same level as that between views #3 and #5. This spatial invariance of crosstalk allows us to design a common anti-alias filter for one view and use it for other views.

5.2. Design of anti-alias filter

Thus far we used 1-D notation, but the anti-alias filter we seek is a 2-D structure. A development of 2-D version of the crosstalk-free and crosstalk-aware multiplexing models of Section 3 is only a notation change for orthogonal (separable) 2-D sub-sampling; scalar function arguments, such as n , become vectors. It is more than a simple notation change for non-separable sub-sampling,⁸ the one considered here, but rather than developing new notation we will draw on parallels between 1-D and 2-D cases to design the anti-alias filters.

Using the crosstalk measurements from previous section and sampling structures of individual views, we can re-create a sampling structure perceived by viewer on the screen in presence of crosstalk. We shall call such a structure the *perceived* sampling structure.

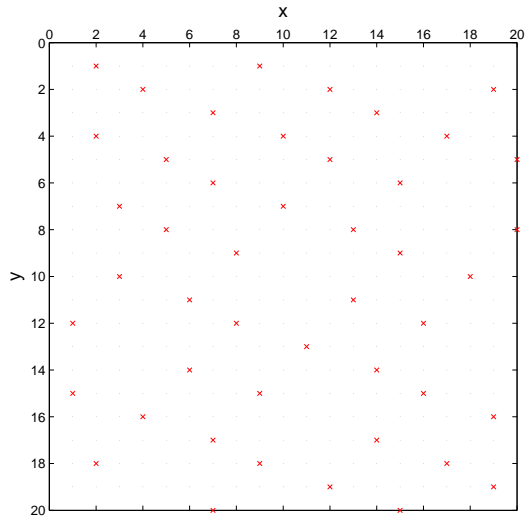
The 2-D sampling structure for red component of view #1, that corresponds to the 1-D train of impulses $x[n]$ (Fig. 1(a) and equation (1)), is shown in Fig. 5(a). Note the irregular nature of the sub-sampling needed to produce red sub-pixels of view #1. Taking the discrete-space Fourier transform of this structure results in a *modulated* 2-D train of impulses (Fig. 6(a)); the impulses are of varying height because of the irregular nature of the sub-sampling pattern.⁸

Similarly, the perceived 2-D sampling structure for red component of view #1 in case with crosstalk, that corresponds to the 1-D train of impulses $x_{all}[n]$ (Fig. 1(b) and equation (3)), is shown in Fig. 5(b). In addition to the irregular nature of the sub-sampling, the amplitude of impulses varies. The discrete-space Fourier transform of this structure is again a *modulated* 2-D train of impulses (Fig. 6(b)).

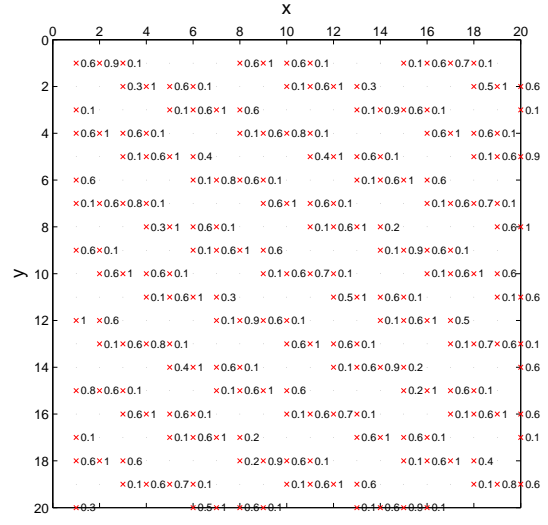
In Fig. 6, the Voronoi cells at DC indicate the passband of the optimal anti-alias filter in each case, when repeat spectra have the same gains (maximum amplitude). Note, however, that these gains actually vary for different spectral replications. In order to find the optimal anti-alias filter we need again to model the views. We use the exponential autocorrelation model discussed in Section 4 but we apply it now in both horizontal and vertical directions thus creating a 2-D separable autocorrelation model $R_u[m, n] = \rho^{|m|}\rho^{|n|}$, whose power spectral density is:

$$\Phi(f_x, f_y) = \frac{1}{\pi^2} \frac{f_0^2}{(f_x^2 + f_0^2)(f_y^2 + f_0^2)}.$$

Since, due to convolution (7), the power spectral density $\Phi(f_x, f_y)$ is repeated at all impulse locations in the frequency domain (Fig. 6), overlaps are unavoidable and the goal, similarly to the 1-D case, is to establish a

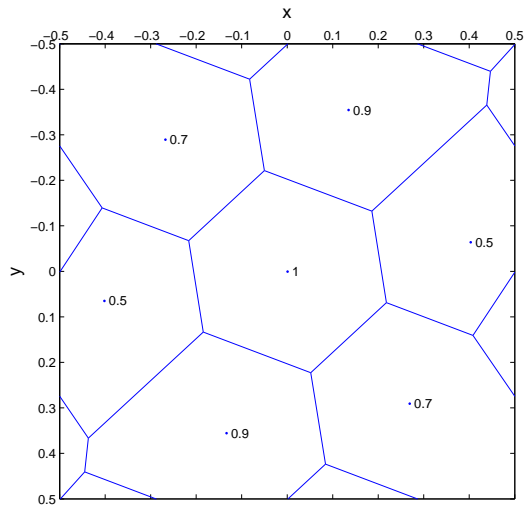


(a)

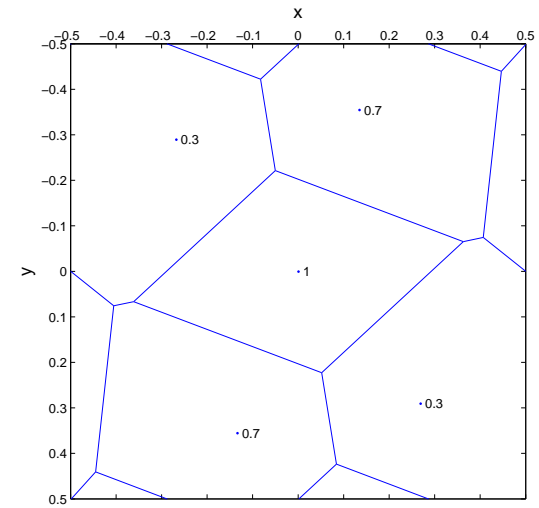


(b)

Figure 5. (a) Sampling structure for red component of view #1 in absence of crosstalk, i.e., locations of 2-D train of unit impulses that multiply view #1 to accomplish the desired sub-sampling; (b) perceived sampling structure for red component of view #1 in presence of crosstalk measured in Section 5.1. Numbers next to sample locations indicate the associated crosstalk ratio. For visual clarity, only neighboring-view samples with crosstalk ratio of 0.1 or more are shown.



(a)



(b)

Figure 6. Discrete-space Fourier transform of: (a) 2-D train of unit impulses from Fig. 5(a) for the crosstalk-free model; and (b) 2-D train of varying-amplitude impulses from Fig. 5(b). For visual clarity, only locations of spectral replications with gain of 0.2 or more are shown and used to compute the Voronoi diagram. Numbers next to sample locations indicate the amplitude of associated impulse.

condition on frequency that limits aliasing without unduly removing image detail. Unlike in 1-D case, however, more than one repeat power spectral density can contribute to a particular baseband frequency; in 1-D case, additional repeat spectra were at least twice further away from baseband thus making their contribution negligible. This is an example of increased complexity of analysis of 2-D systems as compared to 1-D systems.

Since a general analytic expression for the boundary of 2-D anti-alias filter passband is not possible, we determine the boundary (cut-off) frequencies numerically as frequencies at each original spectral energy equals the sum of all repeat spectral energies. This leads to the following specification of the ideal anti-alias filter frequency response:

$$H_{ideal}(f_x, f_y) = \begin{cases} 1, & \text{if } \Phi(f_x, f_y) > K \sum_i \alpha_i \Phi(\xi_x^i - f_x, \xi_y^i - f_y) \\ 0, & \text{otherwise} \end{cases} \quad (12)$$

where (ξ_x^i, ξ_y^i) is the frequency at which i -th spectral replication occurs, and α_i is the associated gain (number in Fig. 6(b)). The constant K permits us to change the passband of the filter. In the experiments, we used $K = 1$.

For the design of 2-D anti-alias filters with the above ideal frequency response specification, we used *MATLAB* function `fwind1` that applies inverse Fourier transform and windowing. We used the Hamming window, for its excellent frequency characteristics, to design 51×51 -coefficient filters.

First, we designed an anti-alias filter assuming no crosstalk between views. Fig. 7(a) shows the desired passband (shaded) as well as the contour plot of the designed filter's magnitude response. Note a fairly accurate match between the 0.7 (-3dB) contour line and the desired passband boundary; while the desired passband area is 0.0912, the designed filter's passband area is 0.0940.

The designed filter is highly restrictive for diagonal frequencies, whereas it allows most of the purely horizontal and vertical frequencies to pass through. The filter's passband area of 0.0912 (1/10.96) is less than 0.1111 (= 1/9) as would be expected from 1:9 sub-sampling. This is because of irregular pixel distribution in individual views of the display. Although frequency restriction occurs mainly diagonally, it is unlikely to be perceived by viewers since spatial contrast sensitivity of the human eye is reduced by about 20% for diagonal gratings.

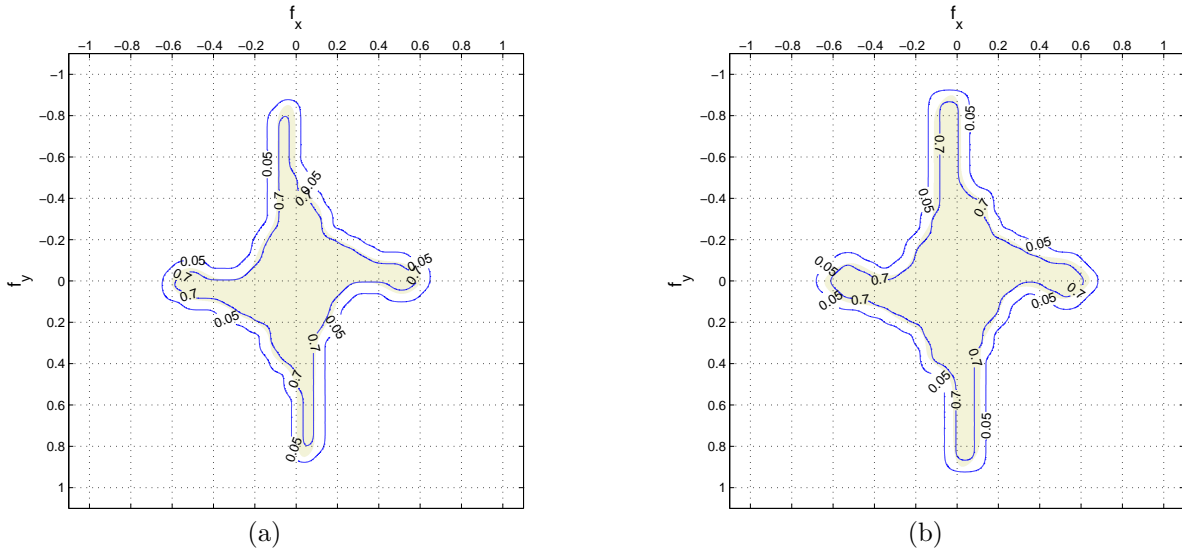


Figure 7. Desired (shaded) and designed (contours) magnitude response of anti-alias filter for multiplexing model: (a) without crosstalk, and (b) with crosstalk. Both frequency axes are normalized to the Nyquist frequency.

Then, we designed an anti-alias filter for the model with crosstalk between views based on crosstalk measurements from Section 5.1. Again, the shaded region in Fig. 7(b) shows the desired passband, while the contours show magnitude response of the designed filter at amplitudes of 0.7 and 0.05. The desired filter passband has

area of 0.1207. The effective passband area, in which magnitude response is greater than 0.707 (half energy point), for the designed 2-D FIR filter is 0.1182, again a very close match to the desired specifications.

Note that the filter designed for the multiplexing model with crosstalk has a larger passband area; the area of $0.1207=1/8.29$ is 32% more than the $0.0912=1/10.96$ area for the crosstalk-free model. The filter, as in the case of no crosstalk, is highly restrictive diagonally but allows purely horizontal and vertical frequencies up to about 0.6 and 0.8 of the Nyquist frequency, respectively. This means that although we are sub-sampling each view by a factor of 9 on average, the loss of frequency would be only 20% purely vertically and 40% purely horizontally.

In comparison with prior work on the design of anti-alias filters for lenticular displays using non-orthogonal lattice approximations,^{7,8} the results presented here rank favorably. Fig. 8(a) shows the passband of an ideal anti-alias filter designed using a non-orthogonal lattice model (no crosstalk). The filter has hexagonal passband of slightly larger area (0.1343) than that of both filters designed here but it restricts spatial frequencies almost equally in all directions. Fig. 8(b) shows the desired passband derived for a union-of-cosets model (no crosstalk). This model approximates sub-sampling of each view using a union of 20 shifted non-orthogonal lattices (cosets). In this case, the ideal filter passband is coarsely hexagonal but very restrictive in purely vertical direction. Moreover, its bandwidth is much smaller than that of the filters designed here (note the frequency scale).

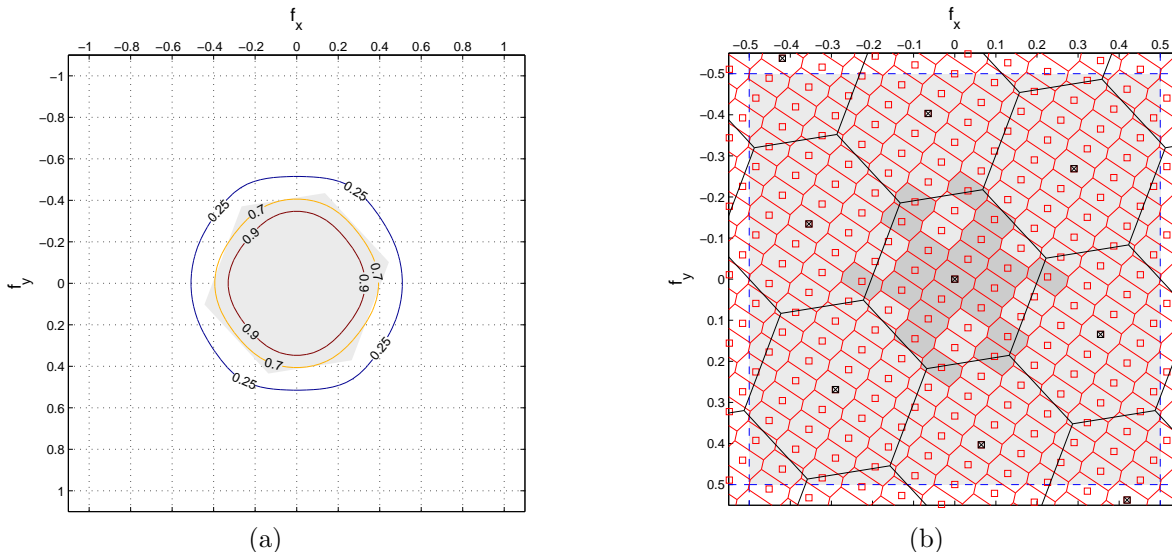


Figure 8. (a) Desired (shaded) and designed (contours) magnitude response of anti-alias filter for a multiplexing model based on non-orthogonal lattice; and (b) desired response for model based on union of cosets (zoomed in be a factor of 2).

5.3. Subjective evaluation

The evaluation of impact of the designed anti-alias filters on perceived 3-D quality was performed by informal subjective viewing. The following defects can be observed when multiplexing is performed without anti-alias pre-filtering: appearance of red, green or blue isolated dots at high-contrast edges, jagged edges at sharp intensity transitions, Moiré patterns, appearance of granular noise in low-texture areas. Both filters designed here, namely disregarding crosstalk and accounting for crosstalk, provided clear improvements. In all tested images, a clear reduction of the visibility of isolated color dots, reduction of edge jaggedness, improvement of textures was observed. More importantly, however, we observed that, as expected, the filter designed based on the multiplexing model aware of crosstalk resulted in visibly improved horizontal and vertical detail with a minimal loss of diagonal detail. This experimentally confirmed that accounting for crosstalk in the theoretical multiplexing model leads to wider anti-alias filter bandwidths and improved detail rendering of 3-D images.

6. CONCLUSIONS

In this paper, we set out to explore the issue of optical crosstalk in spatially-multiplexed automultiscopic 3-D displays and its impact on the design of anti-alias filters needed for view multiplexing. Although optical crosstalk induces ghosting at the boundaries of high-contrast objects with non-zero screen parallax, and may lead to difficulties with 3-D fusion, eye strain, even headaches, it also results in increased perceived 3-D screen brightness and resolution. These facts have been well-known to date. Here we have demonstrated that by incorporating crosstalk into the view multiplexing model, the resulting anti-alias filters have larger passband compared to crosstalk-free models. This, in turn, leads to a better preservation of detail in perceived 3-D images.

7. ACKNOWLEDGMENTS

This work was supported in part by the National Science Foundation (NSF) under Grant ECS-0219224.

REFERENCES

1. A. Woods and S. Tan, "Characterising sources of ghosting in time-sequential stereoscopic video displays," in *Proc. SPIE Stereoscopic Displays and Applications*, **4660**, pp. 66–77, Jan. 2002.
2. J. Lipscomb and W. Wooten, "Reducing crosstalk between stereoscopic views," in *Proc. SPIE Stereoscopic Displays and Virtual Reality Systems*, **2177**, pp. 92–96, Feb. 1994.
3. J. Konrad, B. Lacotte, and E. Dubois, "Cancellation of image crosstalk in time-sequential displays of stereoscopic video," *IEEE Trans. Image Process.* **9**, pp. 897–908, May 2000.
4. S. Klimenko, P. Frolov, L. Nikitina, and I. Nikitin, "Crosstalk reduction in passive stereo-projection systems," in *Proc. EUROGRAPHICS*, pp. 235–240, 2003.
5. C. Van Berkel and J. A. Clarke, "Characterization and optimisation of 3D-LCD module design," in *Proc. SPIE Stereoscopic Displays and Virtual Reality Systems*, **3012**, pp. 179–187, 1997.
6. J. Konrad and P. Agniel, "Artifact reduction in lenticular multiscopic 3-D displays by means of anti-alias filtering," in *Proc. SPIE Stereoscopic Displays and Virtual Reality Systems*, **5006**, pp. 336–347, Jan. 2003.
7. J. Konrad and P. Agniel, "Non-orthogonal sub-sampling and anti-alias filtering for multiscopic 3-D displays," in *Proc. SPIE Stereoscopic Displays and Virtual Reality Systems*, **5291**, pp. 105–116, Jan. 2004.
8. J. Konrad and P. Agniel, "Subsampling models and anti-alias filters for 3-D automultiscopic displays," *IEEE Trans. Image Process.* **15**, pp. 128–140, Jan. 2006.
9. N. Dodgson, "Autostereoscopic 3-D displays," *IEEE Computer* **38**, pp. 31–36, Aug. 2005.
10. C. Van Berkel, A. Franklin, and J. Mansell, "Design and applications of multiview 3D-LCD," in *Proc. SID Euro-Display '96*, pp. 109–112, 1996.
11. <http://www.3dsolutions.philips.com>.
12. L. Lipton and M. Feldman, "A new stereoscopic display technology: The SynthaGram," in *Proc. SPIE Stereoscopic Displays and Virtual Reality Systems*, **4660**, pp. 229–235, Jan. 2002.
13. A. Schmidt and A. Grasnich, "Multi-viewpoint autostereoscopic displays from 4D-Vision," in *Proc. SPIE Stereoscopic Displays and Virtual Reality Systems*, **4660**, pp. 212–221, Jan. 2002.
14. <http://www.newsight.com>.
15. C. Van Berkel, D. W. Parker, and A. R. Franklin, "Multiview 3D-LCD," in *Proc. SPIE Stereoscopic Displays and Virtual Reality Systems*, **2653**, pp. 32–39, 1996.
16. D. Winnek, "Composite stereography." US patent no. 3,409,351, Nov. 1989.
17. C. Van Berkel, "Image preparation for 3D-LCD," in *Proc. SPIE Stereoscopic Displays and Virtual Reality Systems*, **3639**, pp. 84–91, 1999.
18. J. Woods, *Multidimensional Signal, Image and Video Processing and Coding*, Academic Press, 2006.
19. S. Mitra, *Digital Signal Processing: A Computer-Based Approach*, McGraw Hill, 3rd ed., 2006.
20. A. Jain, *Fundamentals of Digital Image Processing*, Information and System Sciences Series, Prentice Hall, 1989.